Finite element
upscaling to
characterize the
seismic response
of hydrocarbon
reservoirs

Juan E. Santos,

Numerical Applied
Geophysics

Finite element upscaling to characterize the seismic response of hydrocarbon reservoirs

ICIAM 2019, July 19th, 2019, Valencia Spain, July 19th

Juan E. Santos,

Universidad de Buenos Aires (UBA), Instituto del Gas y del Petróleo (IGPUBA), Argentina, Department of Mathematics, Purdue University, West Lafayette, Indiana, USA, and School of Earth Sciences and Engineering, Hohai University, Nanjing, 211100, China
Collaborators: J. M. Carcione (OGS), G. B. Savioli (IGPUBA) and P. M. Gauzellino, Universidad Nacional de La Plata

July 8, 2019

- Hydrocarbon Reservoir Formations are fluid-saturated poroelastic media.

- Seimic waves generated near the earth surface or inside wells are used to detect and characterize these formations.

- Biot's theory (1962) descrires the propagation of waves in a poroelastic medium saturated by a single-phase fluid (a Single Phase Biot medium, SPBM).

- Biot's theory predics the existence of two compressional waves (fast (P1) and slow (P2)) and one shear wave (fast S).

Finite element upscaling to characterize the seismic response of hydrocarbon reservoirs

Juan E. Santos,

Numerical Applied Geophysics

- P1 or S-waves travelling through a SPBM containing heterogeneities at the mesoscopic scale suffer attenuation and dispersion observed in seismic data (mesoscopic loss).

- The mesoscopic-scale is larger than the grain sizes but much smaller than the wavelength of the pulse.

- The mesoscopic loss effect occurs because different regions of the medium may undergo different strains and fluid pressures.

- This in turn induces fluid flow and Biot slow waves (WIFF) causing energy losses and velocity dispersion due to energy transfer between wave modes.

Finite element upscaling to characterize the seismic response of hydrocarbon reservoirs

Juan E. Santos,

Numerical Applied Geophysics

- For poroelastic medium saturated by a two-phase fluid (a two-phase Biot medium - 2PBM), capillary forces and interference between the two fluids as they flow within the pore are included in a generalization of Biot's theory for a 2PBM appeared in (JASA, 1990, 2003).

- The theory for a 2PBM predicts the existence of one fast (P1), two slow (P2, P3) compressional waves and one shear (S) wave.

- Capillary forces are responsible for the existence of one additional slow wave and relative permeability functions model energy losses due to interferences between the two fluids as they flow, modifying the (WIFF) mechanism.

Finite element upscaling to characterize the seismic response of hydrocarbon reservoirs

Juan E. Santos,

Numerical Applied Geophysics

In a 2PBM we have *wetting* and *non-wetting* fluid phases and a solid phase, denoted with the subscripts (or superscripts) "w", "n" and "s", respectively.

S_l, S_{rl}: saturation and residual saturation of the l-phase, $l = n, w$. $S_{rn} < S_n < 1 - S_{rw}$.

Assumption:, $S_w + S_n = 1$.
Relative fluid displacements:

$$\mathbf{u}^\ell = \phi(\tilde{\mathbf{u}}^\ell - \mathbf{u}^s), \, \xi^\ell = -\nabla \cdot \mathbf{u}^\ell, \, \ell = n, w.$$

ϕ : matrix effective porosity.

$\mathbf{u}^s = (u_i^s)$, $\tilde{\mathbf{u}}^l = (\tilde{u}_i^l)$ $\ell = n, w$, $i = 1, 2, 3$: time Fourier transforms of the displacement of the solid and fluid phases.

Finite element upscaling to characterize the seismic response of hydrocarbon reservoirs

Juan E. Santos,

Numerical Applied Geophysics

$\tau = \tau_{ij}$, $\varepsilon = \varepsilon_{ij}$, $i, j = 1, 2, 3$: time Fourier transforms of the stress and strain tensors, respectively,

P_l: time Fourier transform of the infinitesimal change in the pressure of the l-fluid phase, taken with respect to the reference value $\bar{P}_l$ $l = n, w$.

This reference value is associated with the initial equilibrium state having non-wetting fluid saturation $\bar{S}_n$ and porosity $\bar{\phi}$.

Capillary relation

$$P_{ca} = P_{ca}(S_n + \bar{S}_n) = \bar{P}_n + P_n - (\bar{P}_w + P_w)$$
$$= P_{ca}(\bar{S}_n) + P_n - P_w \geq 0.$$

The stress-strain relations in a 2PBM:

$$\tau_{ij}(\mathbf{u}) = 2N\,\varepsilon_{ij} + \delta_{ij}(\lambda_u\,e^s - B_1\,\xi^n - B_2\,\xi^w),$$

$$\mathcal{T}_n(\mathbf{u}) = \left(\bar{S}_n + \beta + \zeta\right)P_n - (\beta + \zeta)\,P_w$$

$$= -B_1\,e^s + M_1\,\xi^n + M_3\,\xi^w,$$

$$\mathcal{T}_w(\mathbf{u}) = \left(\bar{S}_w + \zeta\right)P_w - \zeta\,P_n = -B_2\,e^s + M_3\,\xi^n + M_2\,\xi^w,$$

$$\beta = \frac{P_{ca}(\overline{S}_n)}{P'_{ca}(\bar{S}_n)}, \quad \zeta = \frac{\overline{P_w}}{P'_{ca}(\bar{S}_n)}.$$

τ, $\mathcal{T}_n$, $\mathcal{T}_w$: generalized forces in a 2PBM.

Finite element upscaling to characterize the seismic response of hydrocarbon reservoirs

Juan E. Santos,

Numerical Applied Geophysics

The diffusive equations for a 2PBM:

$$\frac{\partial \tau_{ij}}{\partial x_j} = 0,$$

$$i\omega \, (\bar{S}_n)^2 \frac{\eta_n}{\kappa K_{rn}(\bar{S}_n)} \, u_j^n - i\omega \, d_{nw} \, u_j^w + \frac{\partial \mathcal{T}_n}{\partial x_j} = 0,$$

$$i\omega \, (\bar{S}_w)^2 \frac{\eta_w}{\kappa K_{rw}(\bar{S}_w)} \, u_j^w - i\omega \, d_{nw} \, u_j^n + \frac{\partial \mathcal{T}_w}{\partial x_j} = 0, \quad j = 1, 2, 3$$

$$d_{nw}(\bar{S}_n, \bar{S}_w) = \epsilon \left((\bar{S}_n)^2 \frac{\eta_n}{\kappa K_{rn}(\bar{S}_n)} \right) \left((\bar{S}_w)^2 \frac{\eta_w}{\kappa K_{rw}(\bar{S}_w)} \right).$$

η_n, η_w; fluid viscosities
$\kappa, \, K_{rn}(S_n), K_{rw}(S_w)$; the absolute and relative permeabilities.

Choice of relative permeability and capillary pressure functions:

$$K_{rn}(S_n) = (1 - (1 - S_n)/(1 - S_{rn}))^2,$$
$$K_{rw}(S_n) = ([1 - S_n - S_{rw}]/(1 - S_{rw}))^2,$$
$$P_{ca}(S_n) = A\left(1/(S_n + S_{rw} - 1)^2 - S_{rn}^2/[S_n(1 - S_{rn} - S_{rw})]^2\right)$$

A: Capillary pressure amplitude, chosen to be 30 kPa.

Finite element upscaling to characterize the seismic response of hydrocarbon reservoirs

Juan E. Santos,

Numerical Applied Geophysics

- Most shale reservoir rocks are laminated media of very low permeability composed of illite-smectite layers and organic matter in the form of oil, gas and kerogen.

- For seismic wavelengths much larger than the average layer thickness, these materials behave as homogeneous viscoelastic transversely isotropic (VTI) media.

- We define a set of five harmonic experiments to determine the stiffness coefficients of a VTI medium long-wave equivalent to a densely fractured 2PBM.

- The experiments are formulated as boundary value problems (BVP) in the space-frequency domain that are solved using the finite element method (FEM). |

Finite element upscaling to characterize the seismic response of hydrocarbon reservoirs

Juan E. Santos,

Numerical Applied Geophysics

- Since extremely fine meshes are needed to represent mesoscopic-scale heterogeneities (both for SPBM and 2PBM) numerical simulations of wave propagation are computationally expensive or not feasible.

- Alternative: In the context of Numerical Rock Physics, perform five time-harmonic experiments to compute the stiffness coefficients of a VTI medium long-wave equivalent to a densely laminated and highly heterogeneous 2PBM.

- This VTI medium has, in the average, the same attenuation and velocity dispersion than the highly heterogeneous Biot medium.

Finite element upscaling to characterize the seismic response of hydrocarbon reservoirs

Juan E. Santos,

Numerical Applied Geophysics

- Each experiment is associated with a Boundary Value Problem (BVP) that is solved using the FEM.

- In many circumstances Numerical Rock Physics offer an alternative to laboratory measurements. Numerical experiments are inexpensive and informative since the physical process of wave propagation can be inspected during the experiment.

- Moreover, they are repeatable, essentially free from experimental errors, and may easily be run using alternative models of the rock and fluid properties

Finite element upscaling to characterize the seismic response of hydrocarbon reservoirs

Juan E. Santos,

Numerical Applied Geophysics

A 2PBM with a set of horizontal layers behaves as a VTI medium with vertical (x_3) symmetry axis at long wavelengths $\sigma_{ij}(\widetilde{\mathbf{u}}_s)$, $e_{ij}(\widetilde{\mathbf{u}}_s)$: stress and strain tensor components of the VTI medium,

$\widetilde{\mathbf{u}}_s$: solid displacement vector at the macroscale.

The stress-strain relations assuming a closed system:

$$\sigma_{11}(\widetilde{\mathbf{u}}_s) = p_{11}\ e_{11}(\widetilde{\mathbf{u}}_s) + p_{12}\ e_{22}(\widetilde{\mathbf{u}}_s) + p_{13}\ e_{33}(\widetilde{\mathbf{u}}_s),$$

$$\sigma_{22}(\widetilde{\mathbf{u}}_s) = p_{12}\ e_{11}(\widetilde{\mathbf{u}}_s) + p_{11}\ e_{22}(\widetilde{\mathbf{u}}_s) + p_{13}\ e_{33}(\widetilde{\mathbf{u}}_s),$$

$$\sigma_{33}(\widetilde{\mathbf{u}}_s) = p_{13}\ e_{11}(\widetilde{\mathbf{u}}_s) + p_{13}\ e_{22}(\widetilde{\mathbf{u}}_s) + p_{33}\ e_{33}(\widetilde{\mathbf{u}}_s),$$

$$\sigma_{23}(\widetilde{\mathbf{u}}_s) = 2\ p_{55}\ e_{23}(\widetilde{\mathbf{u}}_s),$$

$$\sigma_{13}(\widetilde{\mathbf{u}}_s) = 2\ p_{55}\ e_{13}(\widetilde{\mathbf{u}}_s),$$

$$\sigma_{12}(\widetilde{\mathbf{u}}_s) = 2\ p_{66}\ e_{12}(\widetilde{\mathbf{u}}_s).$$

Note that in a VTI medium $p_{12} = p_{11} - 2p_{66}$,

x_1 and x_3: horizontal and vertical coordinates.
We solve the diffusive equations in the 2D case on a reference square $\Omega = (0, L)^2$ with boundary Γ in the (x_1, x_3)-plane.

Set $\Gamma = \Gamma^L \cup \Gamma^B \cup \Gamma^R \cup \Gamma^T$, where $\Gamma^L, \Gamma^R, \Gamma^B$ and Γ^T denote the left, right, bottom and top boundaries of Ω.

$\{\nu, \chi\}$ the unit outer normal and a unit tangent oriented counterclockwise on Γ

To determine the five p_{IJ} stiffness coefficients, we solve he diffusive equations in Ω with the boundary conditions

$$\mathbf{u}^n \cdot \nu = 0, \quad \mathbf{u}^w \cdot \nu = (x_1, x_3) \in \Gamma, ,$$

and additional boundary conditions for each p_{IJ}.

$$\tau(\mathbf{u})\nu \cdot \nu = -\Delta P, \quad (x_1, x_3) \in \Gamma^T,$$
$$\tau(\mathbf{u})\nu \cdot \chi = 0, \quad (x_1, x_3) \in \Gamma,$$
$$\mathbf{u}^s \cdot \nu = 0, \quad (x_1, x_3) \in \Gamma \setminus \Gamma^T.$$

Using the relation

$$\frac{\Delta V(\omega)}{V} = -\frac{\Delta P}{p_{33}(\omega)}, \tag{1}$$

where V is the original volume of the sample, $p_{33}(\omega)$ can be determined from equation (1) measuring the complex volume change $\Delta V(\omega) \approx L u_{s,3}^{(33,T)}(\omega)$, where $u_{s,3}^{(33,T)}(\omega)$ is the average of the vertical component of the solid phase at the boundary Γ^T.

$$\tau(\mathbf{u})\nu \cdot \nu = -\Delta P, \quad (x_1, x_3) \in \Gamma^R,$$
$$\tau(\mathbf{u})\nu \cdot \chi = 0, \quad (x_1, x_3) \in \Gamma,$$
$$\mathbf{u}^s \cdot \nu = 0, \quad (x_1, x_3) \in \Gamma \setminus \Gamma^R.$$

This experiment determines p_{11} measuring the oscillatory volume change as indicated for p_{33}.

$$\tau(\mathbf{u})\nu \cdot \nu = -\Delta P, \quad (x_1, x_3) \in \Gamma^R \cup \Gamma^T,$$
$$\tau(\mathbf{u})\nu \cdot \chi = 0, \quad (x_1, x_3) \in \Gamma,$$
$$\mathbf{u}^s \cdot \nu = 0, \quad (x_1, x_3) \in \Gamma^L \cup \Gamma^B.$$

From the first and third macroscopic constitutive relations:

$$\sigma_{11} = p_{11}\epsilon_{11} + p_{13}\epsilon_{33} \quad \sigma_{33} = p_{13}\epsilon_{11} + p_{33}\epsilon_{33},$$

ϵ_{11} and ϵ_{33}: the (macroscale) strain components at Γ^L and Γ^T, respectively.

Using that $\sigma_{11} = \sigma_{33} = -\Delta P$, $p_{13}(\omega)$ is determined as

$$p_{13}(\omega) = \frac{p_{11}\epsilon_{11} - p_{33}\epsilon_{33}}{\epsilon_{11} - \epsilon_{33}}.$$

Finite element upscaling to characterize the seismic response of hydrocarbon reservoirs

Juan E. Santos,

Numerical Applied Geophysics

$$-\tau(\mathbf{u})\nu = \mathbf{g}, \quad (x_1, x_3) \in \Gamma^T \cup \Gamma^L \cup \Gamma^R,$$

$$\mathbf{u_s} = 0, \quad (x_1, x_3) \in \Gamma^B,$$

$$\mathbf{g} = \begin{cases} (0, \Delta G), & (x_1, x_3) \in \Gamma^L, \\ (0, -\Delta G), & (x_1, x_3) \in \Gamma^R, \\ (-\Delta G, 0), & (x_1, x_3) \in \Gamma^T. \end{cases}$$

The change in shape of the sample allows to obtain $p_{55}(\omega)$ by using the relation

$$\text{tg}(\beta\omega) = \frac{\Delta G}{p_{55}(\omega)},$$

$\beta(\omega)$: the departure angle between the original positions of the lateral boundaries and those after

applying the shear stresses. $\beta(\omega)$ is determined by measuring the average horizontal displacement at Γ^T.
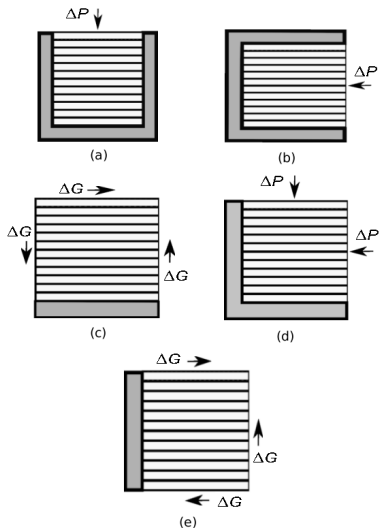
$$-\tau(\mathbf{u})\nu = \mathbf{g}_2, \quad (x_1, x_2) \in \Gamma^B \cup \Gamma^R \cup \Gamma^T,$$
$$\mathbf{u}_s = 0, \quad (x_1, x_2) \in \Gamma^L,$$

$$\mathbf{g}_2 = \begin{cases} (\Delta G, 0), & (x_1, x_2) \in \Gamma^B, \\ (-\Delta G, 0), & (x_1, x_2) \in \Gamma^T, \\ (0, -\Delta G), & (x_1, x_2) \in \Gamma^R. \end{cases}$$

Then, we proceed as indicated for $p_{55}(\omega)$.

Finite element
upscaling to
characterize the
seismic response
of hydrocarbon
reservoirs

Juan E. Santos,

Numerical Applied
Geophysics

Illustration of the five time-harmonic experiments to determine the stiffness coefficients.

Figures 1(a) and 1(b) show how to compute p_{33} and p_{11}, while Figures 1(c) and 1(e) display the experiments determining p_{55} and p_{66}. Figure 1(d) illustrates the experiment to determine p_{13}.

Solution of the BVP's using the FE method. Local DOF.
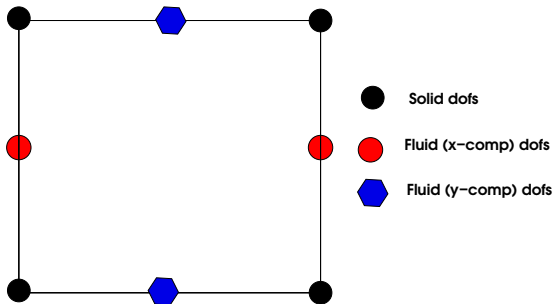
The solution of the time-harmonic tests was computed using the FEM. The figure displays the local degrees of freedom (DOFs) associated with each component of the solid displacement and the fluid displacement vectors. Once we computed the p_{IJ} coefficients, we can determine the velocities and dissipation factors of the equivalent TIV medium.

Finite element upscaling to characterize the seismic response of hydrocarbon reservoirs

Juan E. Santos,

Numerical Applied Geophysics

Complex velocities of the equivalent VTI anisotropic medium:

$$v_{\mathrm{qP}} = (2\bar{\rho})^{-1/2}\sqrt{p_{11}l_1^2 + p_{33}l_3^2 + p_{55} + A},$$

$$v_{\mathrm{qSV}} = (2\bar{\rho})^{-1/2}\sqrt{p_{11}l_1^2 + p_{33}l_3^2 + p_{55} - A},$$

$$v_{\mathrm{SH}} = \bar{\rho}^{-1/2}\sqrt{p_{66}l_1^2 + p_{55}l_3^2},$$

$$A = \sqrt{[(p_{11} - p_{55})l_1^2 + (p_{55} - p_{33})l_3^2]^2 + 4[(p_{13} + p_{55})l_1 l_3]^2}.$$

$\bar{\rho} = \langle \rho \rangle$: average bulk density,

$l_1 = \sin\theta$, $l_3 = \cos\theta$ are the directions cosines, θ is the propagation angle between the wavenumber vector and the x_3-symmetry axis and the three velocities correspond to the qP, qS and SH waves, respectively.

The seismic phase velocity and quality factors are:

$$v_p = \left[\text{Re} \left(\frac{1}{v} \right) \right]^{-1} \quad \text{and} \quad Q = \frac{\text{Re}(v^2)}{\text{Im}(v^2)},$$

where v represents either v_{qP}, v_{qSV} or v_{SH}.

The energy-velocity vector $\mathbf{v}_e$ of the qP and qSV waves is

$$\frac{\mathbf{v}_e}{v_p} = (l_1 + l_3 \cot \psi)^{-1} \hat{\mathbf{e}}_1 + (l_1 \tan \psi + l_3)^{-1} \hat{\mathbf{e}}_3,$$
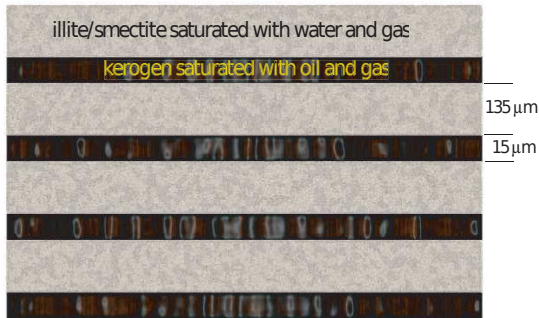
ψ: angle between the energy-velocity vector and the x_3-axis.

The energy velocity of the SH wave is

$$\mathbf{v}_e = \frac{1}{\bar{\rho} v_p} \left(l_1 p_{66} \hat{\mathbf{e}}_1 + l_3 p_{55} \hat{\mathbf{e}}_3 \right).$$

Numerical Experiments. Anisotropy in source rocks.

The FE experiments consider square samples Ω of side length 0.09 cm with 6 alternating layers of illite-smectite saturated with water and gas and kerogen saturated with oil and gas as in the Figure below.

illite/smectite saturated with water and gas

kerogen saturated with oil and gas

$135\,\mu$m

$15\,\mu$m

Schematic model of the Vaca Muerta formation.

Finite element
upscaling to
characterize the
seismic response
of hydrocarbon
reservoirs

Juan E. Santos,

Numerical Applied
Geophysics

Numerical Experiments. Anisotropy in source rocks

The FE experiments consider square periodic layered samples ‰ of side length 0.09 cm with 6 periods of illite-smectite and kerogen layers as in Figure 1 discretized by using a 60×60 uniform mesh. The material properties are given in Table 1.

Table 1. Material Properties.

Property	illite/smectite	kerogen	water	oil	gas
K_s (GPa)	28.4	7	2.25	0.57	0.022
K_m (GPa)	18	4.3	–	–	–
μ_m (GPa)	12.5	1.3	–	–	–
ρ_s (g/cm^3)	2.7	1.4	1	0.7	0.078
ϕ (%)	10	10	–	–	–
η (cP)	–	–	1	10	0.015
κ (ndarcy)	200	200	–	–	–
S_w(%)	99	0	–	–	–
S_o(%)	0	90	–	–	–
S_g(%)	1	10	–	–	–

Finite element upscaling to characterize the seismic response of hydrocarbon reservoirs

Juan E. Santos,

Numerical Applied Geophysics

We consider 6 periods of 0.0135 cm illite-smectite and 0.0015 cm kerogen layers, each layer saturated by a two-phase fluid.
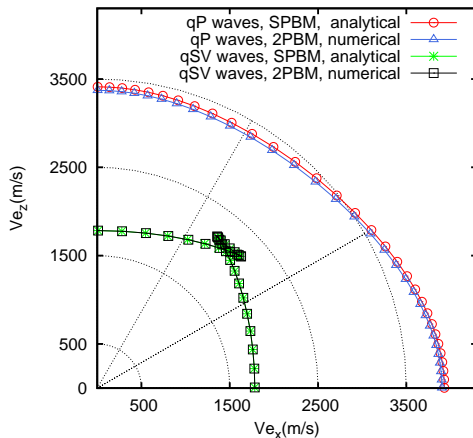
In the illite-smectite layers, the wetting and non-wetting phases are water and gas, with residual saturations $S_{rw} = 4.5\%$ and $S_{rg} = 0$, respectively, and gas saturation is $S_g = 1\%$.

In the kerogen layers, the wetting and non-wetting phases are oil and gas, with residual saturations $S_{rw} = S_{ro} = 4.5\%$ and $S_{rg} = 0$, respectively, and gas saturation is $S_g = 10\%$.
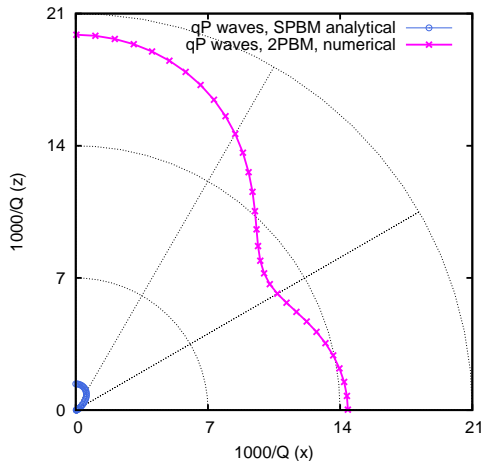
Finite element upscaling to characterize the seismic response of hydrocarbon reservoirs

Juan E. Santos,

Numerical Applied Geophysics

The experiments compare energy velocities and dissipation factors of qP, qSV and SH waves computed by using the 2PBM, when the sample is saturated by a two-phase fluid mixture, with the analytical results for the SPBM given by Krzikalla and Müller (2011).

The effective single phase fluid viscosity $\eta^{(eff)}$, density $\rho^{(eff)}$ and bulk modulus $K^{(eff)}$ used in the SPBM were obtained as Reuss averages for the bulk moduli and arithmetic averages for densities and viscosities:
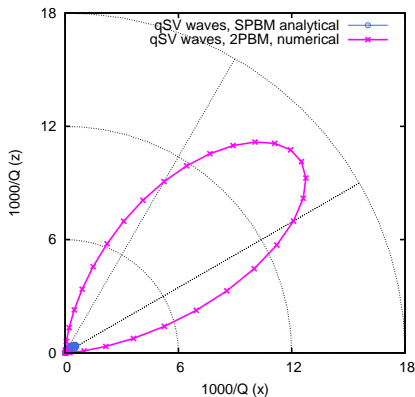
$$\eta^{(eff)} = \eta_n S_n + \eta_w S_w,$$
$$\rho^{(eff)} = \rho_n S_n + \rho_w S_w,$$
$$\frac{1}{K^{(eff)}} = \frac{S_n}{K_n} + \frac{S_w}{K_w}.$$

Finite element
upscaling to
characterize the
seismic response
of hydrocarbon
reservoirs

Juan E. Santos,

Numerical Applied
Geophysics

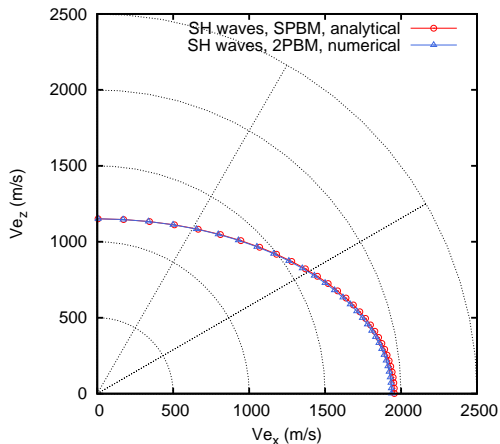**Energy velocities of qP and qSV waves at 50 Hz. Validation. III**

Polar representation of the numerical (FE) energy velocities of qP and qSV waves for the 2PBM and the

corresponding analytical values for the SPBM. Frequency is 50 Hz. The medium is a sequence of nine

water-gas saturated illite-smectite layers and one oil-gas saturated kerogen layer.

Finite element upscaling to characterize the seismic response of hydrocarbon reservoirs

Juan E. Santos,

Numerical Applied Geophysics

Polar representation of the numerical (FE) dissipaton factors of qP waves for the 2PBM and the

corresponding analytical values for the SPBM. Frequency is 50 Hz. The medium is a sequence of nine

water-gas saturated illite-smectite layers and one oil-gas saturated kerogen layer.

Finite element upscaling to characterize the seismic response of hydrocarbon reservoirs

Juan E. Santos,

Numerical Applied Geophysics

Polar representation of the numerical (FE) dissipaton factors of qSV waves for the 2PBM and the corresponding analytical values for the SPBM. Frequency is 50 Hz. The medium is a sequence of nine water-gas saturated illite-smectite layers and one oil-gas saturated kerogen layer.

Finite element upscaling to characterize the seismic response of hydrocarbon reservoirs

Juan E. Santos,

Numerical Applied Geophysics

Polar representation of the numerical (FE) energy velocities of SH waves for the 2PBM and the

corresponding analytical values for the SPBM. Frequency is 50 Hz. The medium is a sequence of nine

water-gas saturated illite-smectite layers and one oil-gas saturated kerogen layer.

Sensitivity to gas saturation in the kerogen layers

We analyzed changes in energy velocities and dissipation factors associated with the amount of gas present in the kerogen layers.

The medium is a sequence of nine water-gas saturated illite-smectite layers and one oil-gas saturated kerogen layer
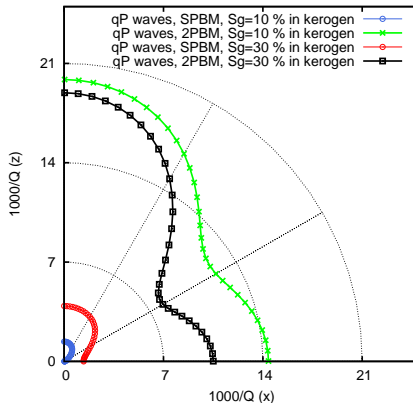
It was observed that energy velocities of qP and qSV waves for a 2PBM (and also for a SPBM) are not sensitive to changes in gas saturation in the kerogen layers.

On the other hand strong differences were observed in the dissipation factors.

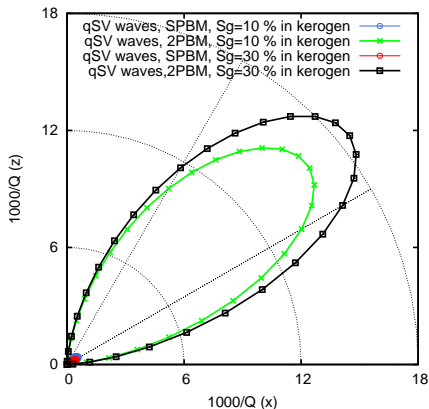Here and in the following experiments $S_{rg} = 0, S_{rw} = 10\,\%$.

Finite element
upscaling to
characterize the
seismic response
of hydrocarbon
reservoirs

Juan E. Santos,

Numerical Applied
Geophysics

Numerical (FE) dissipation factors of qP waves for the 2PBM and the corresponding analytical values for

the SPBM as a function of gas saturation in kerogen layers. Frequency is 50 Hz. The medium is a

sequence of nine water-gas saturated illite-smectite layers and one oil-gas saturated kerogen layer.

Relative permeabilities are responsible for the higher attenuation predicted for the 2PBM as compared

with the SPBM.

Finite element
upscaling to
characterize the
seismic response
of hydrocarbon
reservoirs

Juan E. Santos,

Numerical Applied
Geophysics

Sensitivity to gas saturation in kerogen layers. Dissipation factors of qSV waves at 50 Hz.

Numerical (FE) dissipation factors of qSV waves for the 2PBM and the corresponding analytical values for the SPBM as a function of gas saturation in kerogen layers. Frequency is 50 Hz. The medium is a sequence of nine water-gas saturated illite-smectite layers and one oil-gas saturated kerogen layer. Relative permeabilities are responsible for the higher attenuation predicted for the 2PBM as compared with the SPBM.

Sensitivity to kerogen concentration

We analyzed changes in energy velocities and dissipation factors associated with the amount of kerogen.
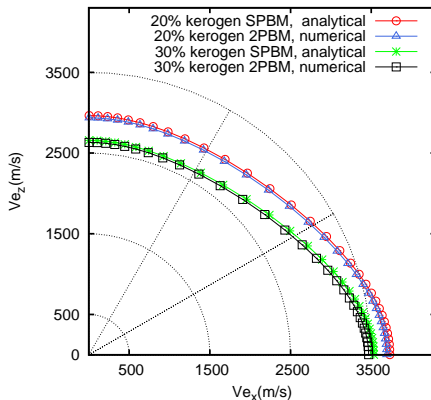
The samples are squares of side length 0.09 cm with 6 periods of 0.012 cm illite-smectite and 0.003 cm kerogen (20% kerogen)

and

6 periods of
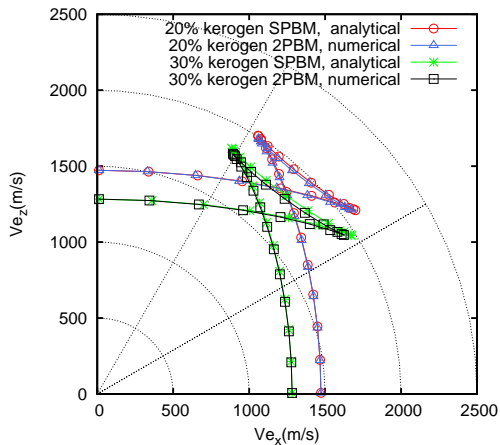0.0105 cm illite-smectite and 0.0045 cm kerogen (30% kerogen).

$S_g = 10\%$ in the illite-smectite and kerogen layers.

Finite element upscaling to characterize the seismic response of hydrocarbon reservoirs

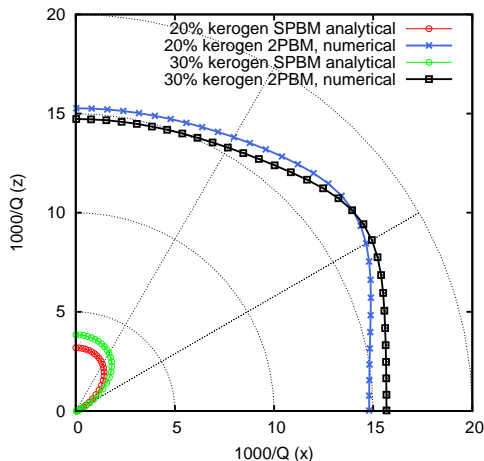Juan E. Santos,

Numerical Applied Geophysics

Numerical (FE) energy velocities of qP waves for the 2PBM and the corresponding analytical values for

the SPBM as a function of kerogen concentration. Frequency is 50 Hz. The medium consists of a

sequence of eight (seven) water-gas saturated illite-smectite layers and two (three) oil-gas saturated

kerogen layer. Lower velocity corresponds to higher kerogen content. Energy velocity values are similar

for the 2PBM and SPBM.

Finite element
upscaling to
characterize the
seismic response
of hydrocarbon
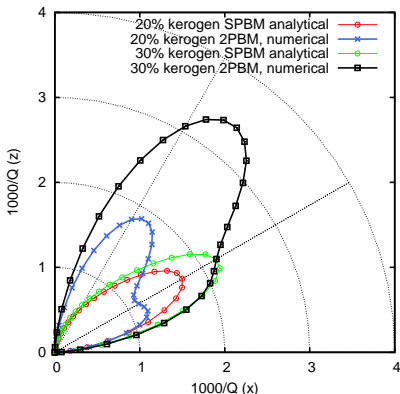reservoirs

Juan E. Santos,

Numerical Applied
Geophysics

Numerical (FE) energy velocities of qSV waves for the 2PBM and the corresponding analytical values for the SPBM as a function of kerogen concentration. Frequency is 50 Hz. The medium consists of a sequence of eight (seven) water-gas saturated illite-smectite layers and two (three) oil-gas saturated kerogen layer. Lower velocity corresponds to higher kerogen content. Energy velocity values are similar for the 2PBM and SPBM.

Finite element
upscaling to
characterize the
seismic response
of hydrocarbon
reservoirs

Juan E. Santos,

Numerical Applied
Geophysics

Sensitivity to kerogen concentration. Dissipation factors of qP waves at 50 Hz.

Numerical (FE) dissipation factors of qP waves for the 2PBM and the corresponding analytical values for the SPBM as a function of kerogen concentration. Frequency is 50 Hz. Dissipation factors are much higher for the 2PBM than for the SPBM. These experiments indicate that the SPBM model is not reliable for predicting attenuation in multiphase saturated porous rocks.

Finite element upscaling to characterize the seismic response of hydrocarbon reservoirs

Juan E. Santos,

Numerical Applied Geophysics

Numerical (FE) dissipation factors of qSV waves for the 2PBM and the corresponding analytical values for the SPBM as a function of kerogen concentration. Frequency is 50 Hz. Dissipation factors are higher and with diffrent anisotropic behavior for the 2PBM than for the SPBM. These experiments indicate that the SPBM model is not reliable for predicting attenuation in multiphase saturated porous rocks.

We analyze the effect of patchy gas-oil saturation in the kerogen layers. Patchy-saturation patterns produce strong mesoscopic-loss effects at the seismic frequency band.
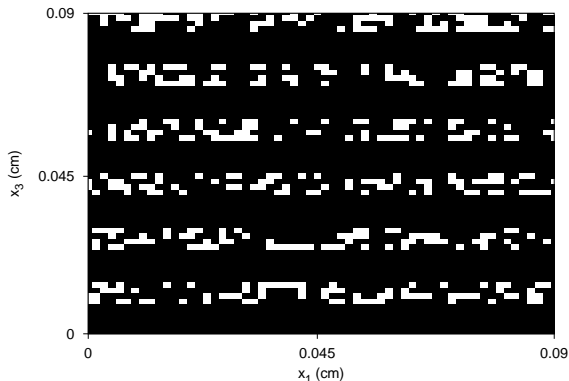
We generate quasi-fractal binary patchy gas-oil distributions using the von-Karman spectral density.

The sample is a square of side length 0.09 cm with a sequence of six water-gas saturated illite-smectite layers and four oil-gas saturated kerogen layer (Kerogen concentration is 40 %).

Saturation in the illite-smectite layers is chosen to be uniform with gas saturation $S_g = 1\%$.

Finite element
upscaling to
characterize the
seismic response
of hydrocarbon
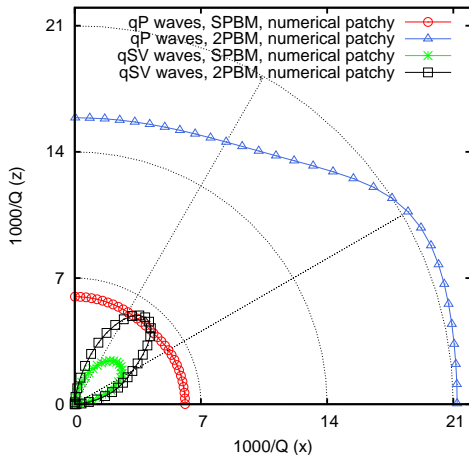reservoirs

Juan E. Santos,

Numerical Applied
Geophysics
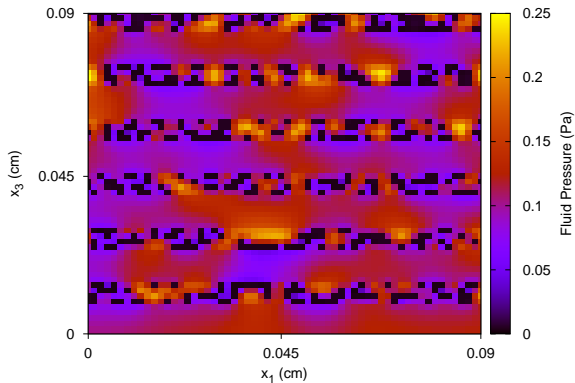
Patchy gas-oil distribution in the kerogen layers.

Patchy gas saturation distribution in the kerogen layers. White regions correspond to $S_g = 30\%$, black regions correspond to $S_g = 1\%$. Overall gas saturation in the kerogen layers is 10 %. The sample is a square of side length 0.09 cm.

Finite element
upscaling to
characterize the
seismic response
of hydrocarbon
reservoirs

Juan E. Santos,

Numerical Applied
Geophysics

Numerical (FE) dissipation factors of the qP and qSV waves for the 2PBM and SPBM at 50 Hz. Patchy gas-oil distribution in the kerogen layers with overall gas saturation $S_g = 10\%$ with . The medium consists of a sequence of six water-gas saturated illite-smectite layers and four oil-gas saturated kerogen layer (Kerogen concentration is 40 %). $S_g = 1\%$ in the illite-smectite layers. Dissipation factors are much higher for the 2PBM than for the SPBM.

Finite element upscaling to characterize the seismic response of hydrocarbon reservoirs

Juan E. Santos,

Numerical Applied Geophysics

Total fluid pressure distribution $\widetilde{\widetilde{\mathcal{T}}} = \widetilde{\widetilde{\mathcal{T}}} = \mathcal{T}_n + \mathcal{T}_w$.

Total pressure gradients are the highest at the gas-oil interfaces. This illustrates the WIFF mechanism.

Finite element
upscaling to
characterize the
seismic response
of hydrocarbon
reservoirs

Juan E. Santos,

Numerical Applied
Geophysics

THANKS FOR YOUR ATTENTION !!!!!!!!